

Progressive Mauve: Multiple alignment of genomes with gene flux and rearrangement

Aaron E. Darling^{1,2,3} Bob Mau⁴

Nicole T. Perna⁵

Running title: Multiple genome alignment

Keywords: Genome Alignment, Genome Rearrangement, pan-genome, core-genome, lateral gene transfer, homologous recombination, population genomics

October 27, 2018

¹Genome Center and Dept. of Computer Science, University of Wisconsin, Madison, WI 53706 USA

²Present address: Institute for Molecular Bioscience, University of Queensland, St. Lucia QLD 4072, Australia

³To whom correspondence should be addressed: darling@cs.wisc.edu

⁴Biotechnology Center and Dept. of Oncology, University of Wisconsin, Madison, WI 53706 USA

⁵Genome Center and Dept. of Genetics, University of Wisconsin, Madison, WI 53706 USA

Abstract

Multiple genome alignment remains a challenging problem. Effects of recombination including rearrangement, segmental duplication, gain, and loss can create a mosaic pattern of orthology even among closely related organisms. We describe a method to align two or more genomes that have undergone large-scale recombination, particularly genomes that have undergone substantial amounts of gene gain and loss (gene flux). The method utilizes a novel alignment objective score, referred to as a sum-of-pairs breakpoint score. We also apply a probabilistic alignment filtering method to remove erroneous alignments of unrelated sequences, which are commonly observed in other genome alignment methods.

We describe new metrics for quantifying genome alignment accuracy which measure the quality of rearrangement breakpoint predictions and indel predictions. The progressive genome alignment algorithm demonstrates vastly improved accuracy over previous approaches in situations where genomes have undergone realistic amounts of genome rearrangement, gene gain, loss, and duplication.

We apply the progressive genome alignment algorithm to a set of 23 completely sequenced genomes from the genera *Escherichia*, *Shigella*, and *Salmonella*. Analysis of whole-genome multiple alignments allows us to extend the previously defined concepts of core- and pan-genomes to include not only annotated genes, but also non-coding regions with potential regulatory roles. The 23 enterobacteria have an estimated core-genome of 2.46Mbp conserved among all taxa and a pan-genome of 15.2Mbp. We document substantial population-level variability among these organisms driven by homologous recombination, gene gain, and gene loss. Interestingly, much variability lies in intergenic regions, suggesting that the Enterobacteriaceae may exhibit regulatory divergence. In summary, the multiple genome alignments generated by our software provide a platform for comparative genomic and population genomic studies.

Free, open-source software implementing the described genome alignment approach is available from <http://gel.ahabs.wisc.edu/mauve>.

INTRODUCTION

Multiple genome alignment is among the most basic tools in the comparative genomics toolbox, however its application has been hampered by concerns of accuracy and practicality (Kumar and Filipinski, 2007, Prakash and Tompa, 2007, Lunter, 2007). Accurate genome alignment represents a necessary prerequisite for myriad comparative genomic analyses.

The definition of a “genome alignment” has been the source of some confusion in comparative genomics. Genome alignment goes beyond basic identification of homologous subsequences to subclassify homology relationships by specific types of evolutionary history (Dewey and Pachter, 2006). At a gross level, subtypes of homology include orthology, paralogy, and xenology (Fitch, 2000). Paralogs can be further classified as in- and out-paralogs, while orthologs can be further distinguished as single-copy orthologs (1-to-1 orthologs), tandemly repeated orthologs (co-orthologs), positional, and general orthologs. For the present work, we are interested in genome alignments that distinguish single-copy orthologous and xenologous sites from the remainder of homologous and unrelated sites. Downstream application of recombination detection methods can distinguish single-copy orthologs from xenologs.

Early genomic studies on *E. coli* revealed substantial gene content variability among individual *E. coli* isolates (Perna et al., 2001, Welch et al., 2002). Since then, gene content variability has been reported as a common feature in numerous other microbial species (Tettelin et al., 2005, Hogg et al., 2007, Hsiao et al., 2005, Vernikos et al., 2007). It appears that microbial populations undergo vast amounts of gene flux and homologous recombination (Mau et al., 2006), although systematic studies have been limited to gene-based methods by the difficulty of complete and accurate multiple genome alignment.

Approaches to whole-genome alignment typically reduce the alignment search space using anchoring heuristics (Ogurtsov et al., 2002, Brudno et al., 2003a, Hohl et al., 2002, Bray and Pachter, 2003, Blanchette et al., 2004) or banded dynamic programming (Chao et al., 1995). Anchoring heuristics appear to provide a good tradeoff between speed and sensitivity. Most anchored alignment methods assume that the input sequences are free from genomic rearrangement. As such, a separate synteny mapping algorithm must be applied to map collinear homologous segments among two or more genomes prior to alignment. Synteny mapping approaches are too numerous to list, however most involve computing reciprocal best BLAST hits on putative ORFs, with BLAST hits filtered by e-value thresholds, coverage thresholds, and uniqueness criteria. Some synteny mapping methods apply genomic context to help resolve ambiguous orthology/paralogy relationships, and others use probabilistic transitive homology approaches to infer orthologs among distantly related taxa (Li et al., 2003).

Integrated approaches to synteny mapping and alignment have been proposed, most of which operate on pairs of genomes (Kurtz et al., 2004, Brudno et al., 2003b, Vinh et al., 2006, Swidan et al., 2006). Research into multiple alignment with rearrangements has been limited, although some progress has been made (Darling et al., 2004a, Treangen and Messeguer, 2006, Raphael et al., 2004, Ovcharenko et al., 2005, Phuong et al., 2006). Apart from greater ease-of-use, integrated synteny mapping and alignment methods have the advantage of providing more accurate inference because the alignment can influence the synteny map and vice-versa.

In the present work, we introduce a novel computational method to construct a multiple alignment of a large number of microbial genomes which have undergone gene flux and rearrangement. Unlike our previous alignment method (Darling et al., 2004a), the new method aligns regions conserved among subsets of taxa. Three algorithmic innovations factor strongly in our method’s ability to align genomes with variable gene content and rearrangement. The first is a novel objective function, called a sum-of-pairs breakpoint score, to score possible configurations of alignment anchors across multiple genomes. Our second algorithmic contribution is a greedy heuristic to optimize a set of anchors under the sum-of-pairs breakpoint score. We demonstrate that most anchored alignment techniques suffer a bias leading to erroneous alignment of unrelated sequence in regions containing differential gene content. Our final algorithmic contribution is application of a homology hidden Markov model (HMM) to reject such erroneous alignments of unrelated sequence.

We compare accuracy of existing methods and the new alignment method on datasets simulated to encompass a broad range of genomic mutation types and rates, including inversion, gene gain, loss, and duplication. We then apply the multiple genome alignment method to a group of 23 finished genomes in the family Enterobacteriaceae (Supplementary Table 1). We precisely identify the core- and pan- genomes of this group, and report basic analysis of gene flux patterns in Enterobacteriaceae.

METHODS

An overview of our method as applied to three hypothetical genomes appears in Figure 1 and is presently described in detail.

Notation and assumptions

Our genome alignment algorithm takes as input a set of G genome sequences $g_1, g_2, \dots, g_G \in \mathbf{G}$. We denote the length of genome i as $|g_i|$. Contigs in unfinished or multi-chromosome genomes are concatenated to form a single coordinate system. Our method computes alignments along a rooted guide tree Ψ which is computed from \mathbf{G} , and we use Ψ_n to denote an arbitrary node in Ψ . As Ψ is a rooted bifurcating tree, an internal node Ψ_n always has two children, which we refer to as $\Psi_n.c_1$ and $\Psi_n.c_2$. Furthermore, we define the set of leaf nodes at or below Ψ_n as $\mathcal{L}(\Psi_n)$. Each leaf node represents a genome from the set of input genomes \mathbf{G} . We use set theoretic notation in some places, where \setminus indicates removal of members from a set.

Various default parameter settings in our software implementation depend on the average length of input genome sequences. We refer to the average genome length as $AvgSize(\mathbf{G})$.

Local multiple alignments as potential anchors

We identify local multiple alignments (LMA) as potential anchors using families of palindromic spaced seed patterns (Darling et al., 2006) in a seed-and-extend hashing method (see Appendix of Darling et al. (2004a)). A spaced seed pattern (Ma et al., 2002) identifies the location of k -mers in the input genomes that have identical nucleotide sequence except that a small number of mutations are allowed at fixed positions. For example, the seed pattern 11*11*11 would identify matching oligomers of length 8 where the 3rd and 6th positions are degenerate. The number of 1's in the seed pattern is commonly referred to as the *weight* of the seed pattern, and a pattern is said to be *palindromic* if the pattern is identical when read forward or in reverse. A seed family is a collection of seed patterns that when used in conjunction provide improved matching sensitivity, and such families have been previously demonstrated to offer excellent speed and sensitivity (Kucherov et al., 2005).

To minimize compute time and focus anchoring coverage on single-copy regions, our method only extends seeds which are unique in two or more genomes. By default, we use seed patterns with weight equal to $\log_2(AvgSize(\mathbf{G})/1.5)$. The resulting local multiple alignments are ungapped and always align a contiguous subsequence of two or more genomes in \mathbf{G} . Any given local multiple alignment m can be described formally by its length $m.Length$ and a tuple $\langle x_1, x_2, \dots, x_G \rangle$ where x_i is an integer denoting the left-end coordinate of the LMA in genome g_i . Genomic coordinates are assumed to start at 1, with negative values denoting alignments to the reverse strand, and when x_i takes on a value of 0, it indicates that genome g_i is not part of the LMA. The LMAs found by our procedure are ungapped alignments of unique subsequences and thus are similar to multi-Maximal-Unique-Matches (multi-MUMs), but may contain mismatches according to the palindromic seed patterns. As with multi-MUMs, any portion of a unique LMA may be non-unique. We refer to the complete set of local multiple alignments generated in this step as \mathbf{M} .

Guide tree construction

We compute a genome-content distance matrix and Neighbor Joining phylogeny using the method described in (Henz et al., 2005), adapted to work on local multiple alignments instead of BLAST

hits. We midpoint-root the resulting tree to yield our progressive alignment guide tree Ψ . Steps 2 and 3 in Figure 1 illustrate guide tree construction.

Local alignment anchor scoring

For a given local multiple alignment m which includes genomes g_i and g_j , we compute a pairwise substitution score using a substitution matrix, which defaults to the HOXD matrix (Chiaromonte et al., 2002). The HOXD matrix appears to discriminate well between homologous and unrelated sequence in a variety of organisms, even at high levels of sequence divergence.

The substitution matrix score quantifies the log-odds ratio that a pair of nucleotides share common ancestry, but does not account for the inherent repetitive nature of genomic sequence. Our desire to discriminate between alignment anchors that suggest orthology (or xenology) and alignments of regions with random similarity or paralogy requires that we somehow consider repetitive genomic sequence in our anchoring score (Lippert et al., 2004). To do so, we compute a quantity termed $S_{occ}(g_i, x)$, which is the number of occurrences in g_i of the spaced seed pattern at site x .

We then combine the traditional substitution score for a pair of nucleotides with an adjustment for the uniqueness of the aligned positions:

$$s(g_i, x, g_j, y) = \begin{cases} Q(g_i, x, g_j, y) & \text{if } Q(g_i, x, g_j, y) \leq 0 \\ \frac{2Q(g_i, x, g_j, y)}{S_{occ}(g_i, x) \cdot S_{occ}(g_j, y)} - Q(g_i, x, g_j, y) & \text{otherwise} \end{cases} \quad (1)$$

where $Q(g_i, x, g_j, y)$ is defined as the substitution matrix score for the nucleotides at sites x of genome g_i and y of g_j . The product of uniqueness scores for the two aligned positions approximates the number of possible ways that repetitive sites could be combined. For example, consider a repeat element present in both genomes with copy number r_i in genome g_i and copy number r_j in g_j . There are $r_i r_j$ possible pairs of repeats. When a pair of nucleotides in a repeat element have a positive substitution score, the product $S_{occ}(g_i, x) \cdot S_{occ}(g_j, y)$ down-weights the score.

We refer to the total pairwise anchor score for match m in genomes g_i and g_j as $S(m, g_i, g_j)$; simply defined as the sum of scores for each alignment column:

$$S(m, g_i, g_j) = \sum_{c=1}^{m.Length} s(g_i, pos(m, g_i, c), g_j, pos(m, g_j, c)) \quad (2)$$

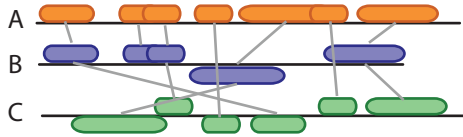
where $pos(m, g_i, c)$ is defined as the position in g_i represented by column c of local alignment m . In summary, the local alignment scoring scheme assigns high scores to well-conserved regions that are unique in each genome and does not consider gap penalties.

Locally collinear blocks

A pair of genomes g_i and g_j may have undergone numerous genomic rearrangements since their most recent common ancestor. As such, local alignments among orthologous segments of g_i and g_j may align segments that occur in a different order or orientation in each genome. We define a pairwise Locally Collinear Block (LCB) as a subset of local alignments in \mathbf{M} that occur in the same order and orientation in a pair of genomes g_i and g_j , i.e. they are free from internal rearrangement. To define pairwise LCBs among genomes g_i and g_j , we first define the projection of the current set of Local Multiple Alignments \mathbf{M} onto g_i and g_j as $\mathbf{M} : \widehat{g_i, g_j}$, computed by setting all left-end coordinates for genomes $\{g_i, g_j\} \setminus \mathbf{G}$ to 0. In alignment m , for example, we would compute the projection onto g_i and g_j by setting all values in the left-end coordinate tuple $\langle x_1, x_2, \dots, x_G \rangle$ to 0 except for x_i and x_j . We can then minimally partition the pairwise alignment projections $\mathbf{M} : \widehat{g_i, g_j}$ into locally collinear blocks using the well-known breakpoint analysis procedure (Darling et al., 2004b, Blanchette et al., 1997). We refer to the minimal partitioning of $\mathbf{M} : \widehat{g_i, g_j}$ into locally collinear blocks as $Lcb(\mathbf{M} : \widehat{g_i, g_j})$, and the resulting subsets of $\mathbf{M} : \widehat{g_i, g_j}$ as $L_{i,j}^1 \cdots L_{i,j}^n \in Lcb(\mathbf{M} : \widehat{g_i, g_j})$.

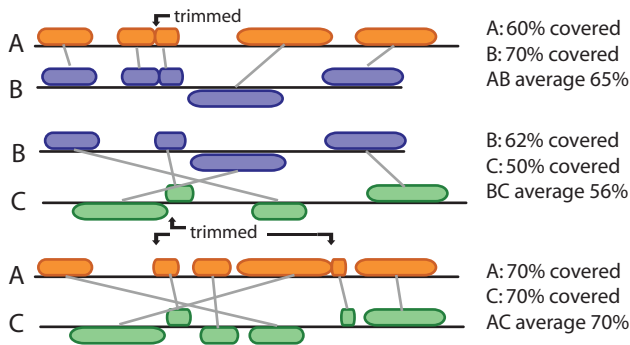
(1) Identify ungapped local multiple alignments

Matches among three genomes (A,B,C) are shown as linked boxes. Matches to a genome's reverse strand are shifted downward



(2) Compute a pairwise distance matrix on single-copy gene content/substitutions

A nucleotide is considered "covered" if it is both contained in a match and identical in the other genome. Overlapping matches are trimmed.

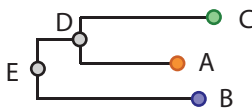


Pairwise coverage values are subtracted from one to yield a distance value. The matrix is used to infer a guide tree and to scale the breakpoint penalty during anchoring.

	A	B	C
A	0	0.35	0.30
B	-	0	0.44
C	-	-	0

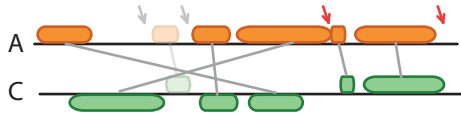
(3) Infer anchoring guide tree on gene content/substitution distances

Use Neighbor-Joining, apply midpoint rooting



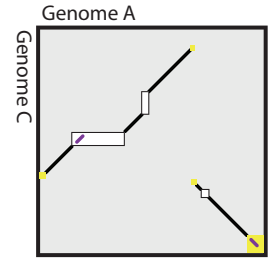
(4) Anchor nearest unaligned sequences in guide tree

A and C are closest. Overlapping matches are trimmed, then we apply sum-of-pairs greedy breakpoint elimination to select anchors (see text). Breakpoints are shown as arrows. Matches in gray were removed, eliminating the breakpoints in gray and improving the Sum-of-pairs anchor score. If the anchor score has not improved after an iteration of step 5, we skip to step 6.



(5) Recursive anchor search

For each pair of genomes regions between anchors (white) and regions outside LCBs (yellow) are searched for new anchors. Newly found anchors are shown in purple. We now return to step 4 (not shown).



(6) Perform global anchored alignment

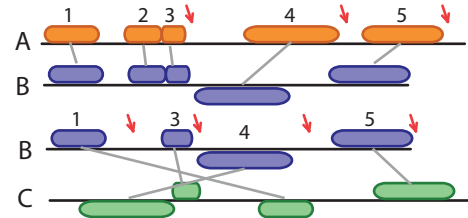
The current set of anchors are used for profile-profile alignment. Inter-anchor regions shown in white and yellow above are aligned.

(7) Evaluate whether all genomes are aligned

Genome B remains unaligned, so return to step 4.

(4.ii) Anchor nearest unaligned sequences in guide tree

A and C are already aligned, so we must align B to D, and use BA and BC anchors to do so. We enforce consistency among anchors and apply greedy breakpoint elimination.



Breakpoints are shown as red arrows, and matches are assigned numeric identifiers. The pairwise LCBs among A,B are: {1,2,3}, {4}, {5}. Pairwise LCBs among B,C are: {1}, {3}, {4}, {5}. The effect of removing matches in each LCB is evaluated with the Sum-of-pairs anchor score, and matches whose removal yields the largest improvement are removed. In this case, the score can not be improved so we continue to step 5.ii.

(5.ii) Recursive anchor search

As above, but among the pairs BA and BC.

(6.ii) Perform anchored alignment with MUSCLE

As above, but among B and the existing AC alignment.

(7.ii) Evaluate whether all genomes are aligned

All genomes are now aligned, continue to step 8.

(8) Reject alignments of unrelated sequence with a Homology HMM

Use the method of Treangen *et al* 2008 to eliminate gap dribble.

Figure 1: Overview of the alignment algorithm using three example genomes A, B, and C.

Sum-of-pairs anchoring objective function

Our method computes alignments progressively according to a guide tree. When computing an alignment at a given internal node of the guide tree Ψ_n , we optimize the following sum-of-pairs LCB anchoring objective function to select a set of alignment anchors:

$$SPAnchorScore(\Psi_n, \mathbf{M}) = \sum_{g_i \in \mathcal{L}(\Psi_n.c_1)} \sum_{g_j \in \mathcal{L}(\Psi_n.c_2)} \left\{ -b|Lcb(\mathbf{M} : \overbrace{g_i, g_j})| + \sum_{m \in \mathbf{M} : \overbrace{g_i, g_j}} S(m, g_i, g_j) \right\} \quad (3)$$

where $|Lcb(\mathbf{M} : \overbrace{g_i, g_j})|$ refers to the total number of LCBs in the set of local alignments among genomes g_i and g_j . The coefficient b is a breakpoint penalty, which when multiplied by the number of LCBs $|Lcb(\mathbf{M} : \overbrace{g_i, g_j})|$, creates a scoring penalty that increases in magnitude when the anchors in $\mathbf{M} : \overbrace{g_i, g_j}$ induce a larger number of LCBs. The value of the breakpoint penalty b is a user-controlled parameter in our implementation of the algorithm, and we use a default value of 30,000 as manual experimentation on real genome sequence data suggests this value represents a good tradeoff between sensitivity to small genomic rearrangements and filtration of spurious alignments. Thus, anchor sets inducing fewer breakpoints are given higher scores.

Optimizing the SP anchoring objective function: greedy breakpoint elimination

We apply a greedy breakpoint elimination heuristic to optimize $SPAnchorScore(\Psi_n, \mathbf{M})$ which removes potential anchors from \mathbf{M} until the score can no longer be increased. Specifically, if all local alignments comprising an LCB $L_{i,j}$ are removed from \mathbf{M} , then the number of LCBs in $Lcb(\mathbf{M}_{i,j})$ will decrease by at least one and at most four if neighboring LCBs coalesce (Darling et al., 2004a). The decreased number of LCBs, and hence breakpoints, reduces the total breakpoint penalty in $SPAnchorScore(\Psi_n, \mathbf{M})$.

Our algorithm repeatedly identifies the LCB whose removal from \mathbf{M} would provide the largest increase to $SPAnchorScore(\Psi_n, \mathbf{M})$ and removes the local alignments which comprise that LCB from \mathbf{M} . This procedure corresponds to step 4 in Figure 1. Formally, we identify $L_{i,j}$ which satisfies:

$$\max_{g_i \in \mathcal{L}(\Psi_n.c_1), g_j \in \mathcal{L}(\Psi_n.c_2)} \left\{ \max_{L_{i,j} \in Lcb(\mathbf{M} : \overbrace{g_i, g_j})} SPAnchorScore(\Psi_n, \mathbf{M} \setminus L_{i,j}) \right\} \quad (4)$$

and remove the local alignments in $L_{i,j}$ from \mathbf{M} . The greedy breakpoint elimination process repeats until further removal of LCBs fails to improve the SP anchoring score.

Recursive anchoring

The initial set of local alignments in \mathbf{M} is typically computed using a seed weight that finds local alignments in unique regions of high sequence identity. As such, the initial set of anchors frequently misses homologous regions with lower sequence identity. After anchor selection by greedy breakpoint elimination (Equation 4), our method searches for additional local alignments between anchors existing among all pairs of genomes in $\mathcal{L}(\Psi_n.c_1)$ and $\mathcal{L}(\Psi_n.c_2)$, see Figure 1 step 5. To improve sensitivity during recursive anchor search, smaller seed weights are used as described by Darling et al. (2004a). Any new local alignments are added to \mathbf{M} . After the recursive anchor search, we apply greedy breakpoint elimination to optimize the SP anchor score once again. The recursive anchoring process repeats until $SPAnchorScore(\Psi_n, \mathbf{M})$ no longer improves.

Anchored profile alignment and iterative refinement

Each LCB at Ψ_n contains alignment anchors, which we use to perform an anchored profile-profile global alignment using modified MUSCLE software (Edgar, 2004). After the initial profile-profile

alignment, we apply window-based iterative refinement to improve the alignment. Step 6 of Figure 1 corresponds to this process. Importantly, MUSCLE attempts to refine the alignment on a multitude of alternative guide trees and is not restricted to the guide tree chosen for progressive anchoring. The use of multiple guide trees is a particularly important feature in microbial genomes, which are subject to extensive lateral gene transfer. It should be noted that our use of MUSCLE as a refinement step is an approach used in other software pipelines as well (Margulies et al., 2007).

Rejecting alignments of unrelated sequences

Segments of DNA between high-scoring alignment anchors are often unrelated, especially in bacteria. Despite that, our method (like most other genome aligners) applies a global alignment algorithm to all inter-anchor segments, naïvely assuming that homology exists. Our assumption of homology often proves erroneous, so to arrive at an accurate alignment we must detect forced alignment of unrelated sequence. To do so, we apply an HMM posterior decoder that classifies columns in a pairwise alignment as either homologous or unrelated. The HMM structure, transition, and emission probabilities are described elsewhere (Treangen et al., 2008). The HMM makes predictions of pairwise homology, which we combine using transitive homology relationships. Regions found to be unrelated are removed from the final alignment. Application of the homology HMM is the final step in the alignment procedure, shown as step 8 in Figure 1.

Implementation

The alignment algorithm has been implemented in the `progressiveMauve` program included with Mauve v2.0 and later. The program is open source C++ code (GPL), with 32- and 64-bit binaries for Windows, Linux, and Mac OS X available from <http://gel.ahabs.wisc.edu/mauve>. Time-consuming portions of the algorithm have been parallelized using OpenMP 2.5 (Chandra et al., 2001). An accessory visualization program is included (see Figure 7). Default alignment parameters have been calibrated for bacterial genomes (Darling, 2006).

RESULTS

Quantifying alignment accuracy

Our new alignment algorithm uses approximations and computational heuristics to compute alignments. To understand the quality of alignments produced by our approach it is essential to objectively quantify alignment accuracy. Without a known ‘correct’ genome alignment, automated alignment heuristics can not be evaluated for accuracy. Although several benchmark data sets exist for protein sequence alignment (Thompson et al., 1999, Edgar, 2004), no such benchmark data sets exist for genome alignment with rearrangement. Thus far, manual curation of a whole-genome multiple alignment that includes rearrangement and lateral gene transfer has proven too time-consuming and difficult. Despite the lack of a manually curated correct alignment, we can estimate the alignment accuracy by modeling evolution and aligning simulated data sets. All results described in this section and the programs used to generate them are available as supplementary material.

Simulated evolution model

In previous work, we constructed a genome evolution simulator that captures the major types, patterns, and frequencies of mutation events in the genomes of Enterobacteriaceae (Darling et al., 2004a). We use the same simulated model of evolution in the present study but with different evolutionary parameters. Given a rooted phylogenetic tree and an ancestral sequence we generate evolved sequences for each internal and leaf node of the tree, along with a multiple sequence alignment of regions conserved throughout the simulated evolution. Along the branches, mutations such as nucleotide substitution, indels, gene gain/loss, and inversion rearrangements are modeled as

a marked Poisson process. We score calculated alignments against the correct alignments generated during the evolution process.

Although gene duplication does occur in bacteria, we do not *explicitly* model it here as duplications tend to be unstable in bacterial chromosomes and are often counterselected (Achaz et al., 2003). Instead, we indirectly account for gene duplications in two ways. First, the source DNA sequence for gene gain events comes from a 1Mbp pool of sequence. At moderate to high simulated rates of gene gain, many megabases of DNA are sampled from the donor pool, and as a result, identical donor sequence gets inserted into the simulated genomes in multiple places. The effect is similar to a dispersed repeat family, such as bacterial IS elements or mammalian SINE elements.

Second, we use the genome sequence of *E. coli* O157:H7 as ancestral sequence and as donor sequence for all insertion and gene gain events. The *E. coli* O157:H7 genome has numerous naturally occurring repeats that are carried on to simulated descendant genomes. By using real genome sequence as ancestral sequence, the resulting evolved genomes often have similar nucleotide, dinucleotide, k -mer composition, repeat copy number and repeat distribution. The unknown natural forces governing the evolution of such traits would otherwise be extremely difficult to capture in a simulation environment.

Our experimental results at high mutation rates should be interpreted with caution, however, since the more simulated mutations applied, the less a simulated genome will look like a real genome.

Accuracy evaluation metrics

Previous studies of alignment accuracy have used a sum-of-pairs scoring scheme to characterize the residue level accuracy of the aligner (Thompson et al., 1999, Darling et al., 2004a). The experiments presented here use sum-of-pairs scoring, but we also define new accuracy measures to quantify each alignment system’s ability to predict indels and breakpoints of genomic rearrangement. For each type of mutation, we define True Positive (TP), False Positive (FP), and False Negative (FN) predictions as discussed below. Using these definitions, we can measure the aligner’s Sensitivity as $\frac{TP}{TP+FN}$ and Positive Predictive Value (PPV) as $\frac{TP}{TP+FP}$.

For nucleotide pairs, a TP is a pair aligned in both the calculated and correct alignments. A FP is a nucleotide pair in the calculated alignment that is absent from the correct alignment. Likewise, a FN is a pair in the correct alignment not present in the calculated alignment. We do not quantify True Negative (TN) alignments as the number of TN possibilities is extremely large, growing with the product of sequence lengths.

We classify each indel in the correct alignment as a TP or a FN based on the predicted alignment. A true positive indel has at least one correctly aligned nucleotide pair in the diagonal/block on either side of the indel and at least one nucleotide correctly aligned to a gap within the indel (see Figure 2). The number of TP indels will never exceed the number of indels in the correct alignment. We define FP indel predictions as the number of excess indel predictions beyond the true positives. FN indels lack a correctly predicted nucleotide pair in the flanking diagonals/blocks or lack predictions of gaps in the correct gapped region. Figure 2 gives examples of each case.

Aligners are notoriously bad at predicting the exact position of indels (Lunter et al., 2008). Under our definition, a TP indel prediction need not predict the exact boundaries of an indel, merely the existence of an indel. This scheme allows us to distinguish cases of missing indel predictions from cases where the indel was predicted but not positioned correctly. We quantify indel boundary prediction accuracy as the distance between the true boundary and the nearest aligned nucleotide pair in the diagonal/blocks which flank the predicted indel. When the predicted indel is too large, our metric assigns a positive value to the boundary score. When the predicted indel is too small, a negative value is assigned.

Large indels have historically caused problems for nucleotide aligners, which have a tendency to break up large indels into a string of smaller gaps with intermittent aligned sequence. Under our definition, a large indel can still be considered as a TP prediction even if it is broken into a string of smaller gaps by the aligner (See Figure 2 prediction A for an example). Our rationale is that the aligner did correctly predict the presence of unrelated sequence, for which it garners a TP, but erroneously predicts additional transitions to and from homology, which are classified as FP

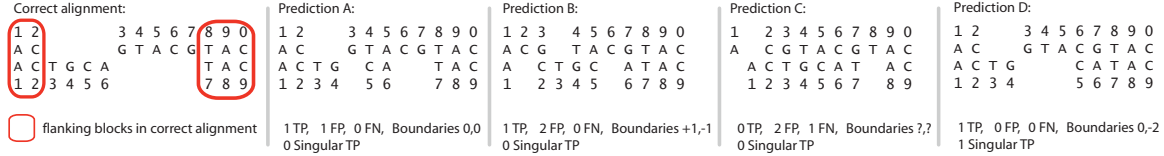


Figure 2: Quantifying indel accuracy. The correct alignment is shown at left and four possible predicted alignments are shown as A, B, C, and D. Nucleotides have been assigned a numerical identifier. The correct alignment has a single indel which partitions the alignment into three sections: the left aligned block, the indel, and the right aligned block. Predicted alignments must have one correctly aligned nucleotide pair in each of the three sections to count a true positive indel prediction.

indel predictions. To distinguish whether a TP indel was broken into two or more smaller gaps, we define a class of “singular” TP indel predictions as indels that were predicted as a single alignment gap. See Figure 2 prediction D for an example of a “singular” TP indel.

For each pair of genomes we also measure whether the aligner correctly predicts LCBs among that pair, yielding a sum-of-pairs LCB accuracy metric. For each pairwise LCB in the true alignment, we record a TP LCB prediction when the predicted alignment contains at least one correctly aligned nucleotide pair in that LCB. Pairwise LCBs lacking any correctly predicted nucleotide pairs are FN predictions. Finally, pairwise LCBs in the predicted alignment lacking any correctly aligned nucleotide pairs are False Positive (FP). Again, we do not measure TN.

As with indels, we define a separate metric to quantify how well each aligner localizes the exact breakpoints of rearrangement. For TP LCB predictions, we record the difference (in nucleotides) between the boundaries of the correct LCB and those of the predicted LCB. The resulting value is negative when the predicted LCB fails to include the full region of homology, and positive when a predicted LCB extends beyond the true boundary.

Under our definitions of TP, FP, TN, and FN predictions, specificity, which is commonly defined as $\frac{TN}{FP+TN}$, is not a useful metric. The extremely large values taken on by TN would drive the quotient to 1 in most cases.

Accuracy on collinear genomes

Our first experiment compares the accuracy of Mauve 1.3.0, Progressive Mauve, MLAGAN 2.0, MAVID 2.0, and TBA 28-02-2006 when aligning collinear sequences that have undergone increasing amounts of nucleotide substitution and indels. For each combination of indel and substitution rate, nine genomes are evolved from a 1Mbp ancestor according to a previously inferred phylogeny (Darling et al., 2004a) shown in Figure 4. We then construct alignments of evolved sequences using each aligner with default parameters, and quantify sensitivity and positive predictive value, (PPV) for nucleotide pair and indel predictions. Three replicates were performed, results shown in Figure 3.

In general, all aligners perform well on collinear sequence, except for Mauve 1.3.0 which is unable to anchor genomes with high mutation rates. Of the tested aligners, TBA offers the highest nucleotide sensitivity, and Progressive Mauve gives the best indel sensitivity and positive predictive value in most cases. Despite that, all aligners are quite bad at predicting indels accurately, which may be in part due to an inherent loss-of-information introduced during the course of simulated evolution (Lunter et al., 2008). We did not test the Pecan aligner here, although a detailed evaluation of its performance can be found elsewhere (Margulies et al., 2007) and we do perform some testing on it below.

Accuracy in the face of rearrangement and gene flux

We assessed the relative performance of Mauve 1.3.0, Progressive Mauve, and TBA (Blanchette et al., 2004) when aligning genomes with high rates of genomic rearrangement, gene flux, and nucleotide substitution. Although the original TBA manuscript did not fully describe alignment

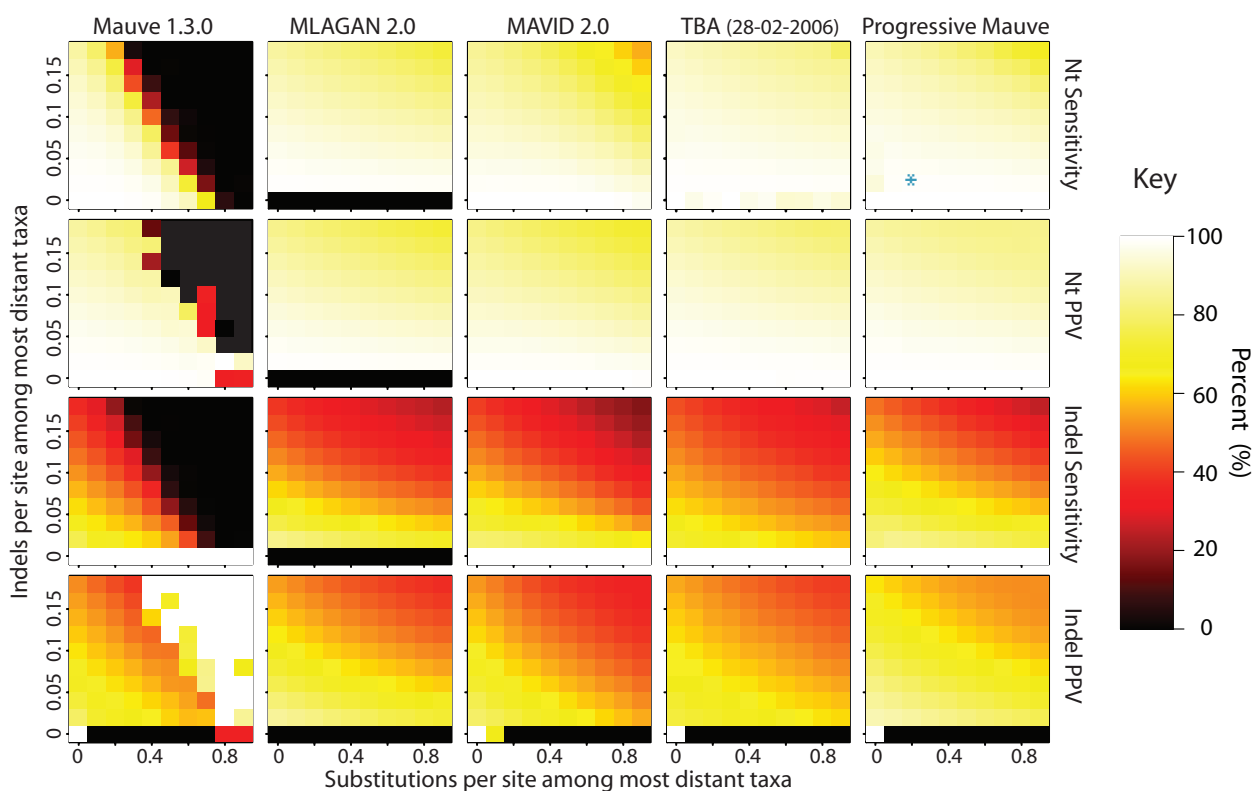


Figure 3: The accuracy of aligners on sequences evolved without rearrangement and with increasing nucleotide substitution and indel rates. Aligners were tested on 100 combinations of indel and substitution rate, with performance averaged over three replicates. All methods lose accuracy as mutation rates grow, and the most accurate alignment method depends on the particular mutation rates. Progressive Mauve and MLAGAN exhibit the best indel sensitivity and positive predictive value (PPV), while TBA is more sensitive than other methods at extremely high mutation rates. MLAGAN did not align genomes without indels within the allotted 10 hours, resulting in the black row at the bottom. The asterisk in this figure indicates the combination of indel rate and substitution rate expected to be similar to our 23 target genomes.

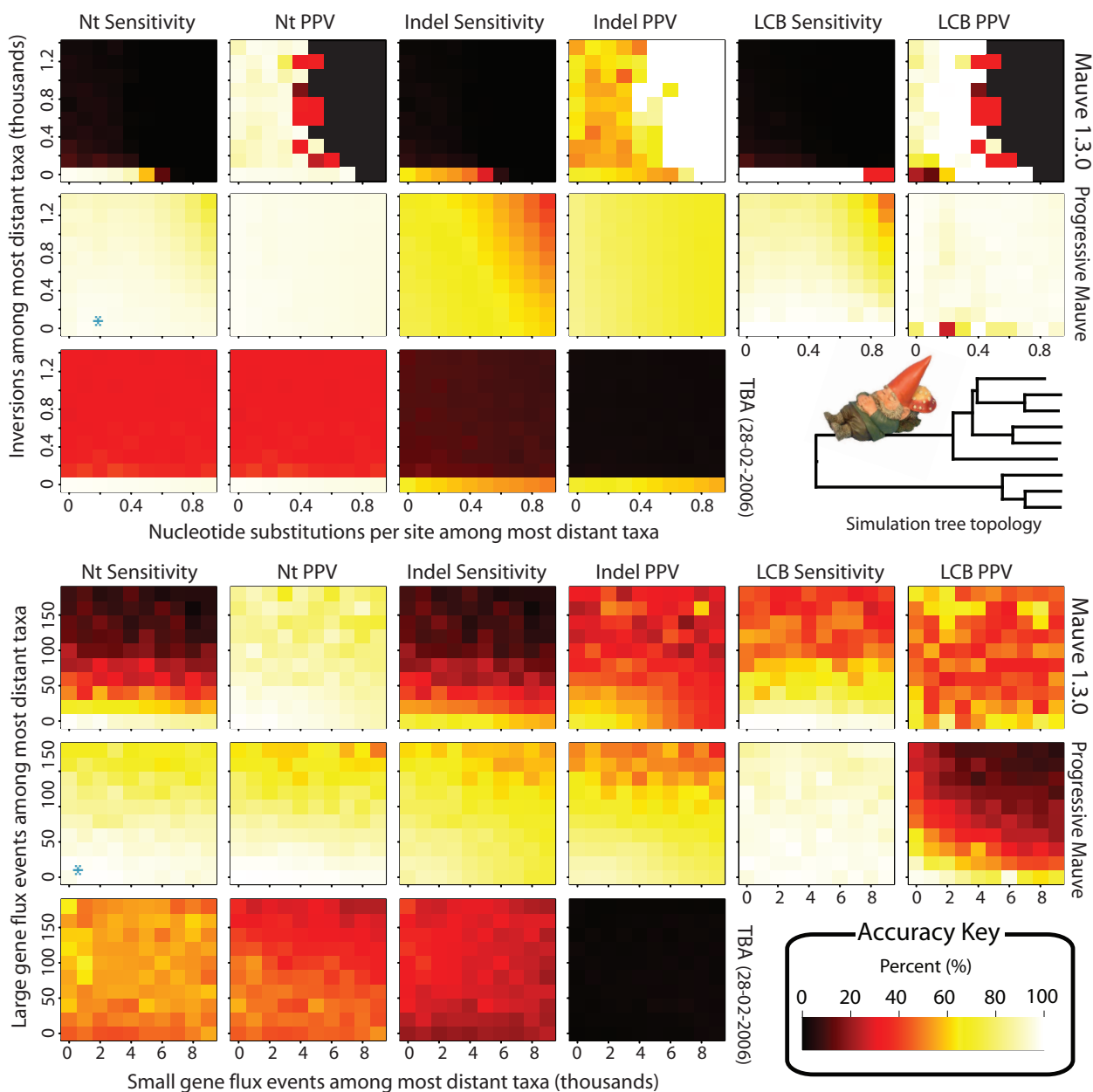


Figure 4: Accuracy of Mauve, Progressive Mauve, and TBA when aligning genomes with inversions and gene flux. In the experiments shown at top, the inversion rate increases along the y -axis and the substitution rate along the x -axis. The most distant taxa have 0.05 indels per site. Progressive Mauve clearly outperforms Mauve 1.3.0 and TBA over the entire space of inversion rates. It should be noted that in the UCSC browser alignments TBA is used in conjunction with a separate synteny-mapping method to identify rearrangements (Miller et al., 2007), so the performance results given here are not cause for alarm. Experiments at bottom quantify aligner performance in the presence of small- and large-scale gene flux (gain/loss) events. The y -axis gives the average number of large gene flux events [length \sim Unif(10kbp, 50kbp)] between the most distant taxa, while the x -axis gives small gene flux events [length \sim Geo(200bp)]. Substitution and indel rates are those indicated by the asterisk in Figure 3, and the most distant taxa have 42 inversions on average. The asterisk in this figure indicates a simulation scenario expected to be similar to our 23 target genomes. Once again Progressive Mauve outperforms other methods, but all methods break down when faced with substantial large-scale gene flux. Of note, when Mauve 1.3.0 attains high PPV it usually does so with very poor sensitivity.

with genomic rearrangement, the most recent release (dated 28-02-2006) handles it (Raphael et al., 2004, Ovcharenko et al., 2005). For our first set of experiments, shown in the top half of Figure 4, we simulated evolution at 100 combinations of substitution and inversion rate. In addition to nucleotide and indel accuracy, we also quantify LCB accuracy on this data set. The results indicate that Progressive Mauve can accurately align genomes with substantially higher rates of rearrangement than other approaches. Although TBA exhibits lackluster performance in comparison to Progressive Mauve, comparison with the results for MAVID 2.0 and MLAGAN 2.0 (shown in Supplementary Figure 8) demonstrates that for all rates of inversion, TBA produces much better alignments than methods which assume genomes are free from rearrangement.

For the second set of experiments we simulated genomes with 10 increasing rates of small-scale gene flux and 10 increasing rates of large-scale gene flux. Small gene flux events are geometrically size distributed with mean 200bp, while large gene flux events have uniform lengths between 10kbp and 50kbp. These sizes were chosen to match empirically derived estimates (Darling et al., 2004a). The results, shown in Figure 4, indicate that Mauve 1.3.0 falters when faced with large-scale gene flux, while Progressive Mauve and TBA perform significantly better. As gene flux rates increase in our model, the amount of orthologous sequence shared among genomes deteriorates, eventually reaching zero in the limit of infinitely high gene flux rates.

Gap dribble and the quality of long gap predictions

Gene gain and loss events manifest themselves in genome alignments as long gaps. Every predicted alignment gap implies at least one insertion or deletion of nucleotides has taken place in the history of the organisms under study. Since we would like to quantify the contribution of gene flux to the target genomes, it is imperative that predicted alignment gaps be as accurate as possible.

Current sequence alignment methods typically score pairwise alignments with an affine gap scoring scheme consisting of a gap open penalty and a gap extend penalty. In a probabilistic setting, the optimal affine-gap alignment corresponds to a viterbi path alignment from a pair-HMM with a single pair of insert and delete states (Durbin et al., 1998). However, when aligning genomes which have undergone a significant amount of gene gain and loss, an excess of large gaps exists that does not fit the gap size distribution imposed by a standard global alignment pair-HMM (Lunter, 2007). The net result is that under the affine gap model, aligners tend to break up large gaps into a series of small gaps interspersed with short stretches of improperly aligned nucleotides. In the spirit of classifying systematic alignment errors introduced by Lunter et al. (2008), we refer to this problem as *gap dribble*, since short alignments are dribbled along the large gap. The large number of small gaps creates problems when trying to reconstruct the history of gene gain and loss events, since they imply a much greater number of insertions and deletions than actually occurred.

Using our simulated evolution platform, we quantify the performance of each aligner in predicting gaps of varying size. We simulated evolution of collinear genomes (no rearrangement) that have undergone a realistic amount of gene gain and loss, corresponding to previous estimates for the rates of these events in the enterobacteria Darling et al. (2004a). Nucleotide substitutions and indels were modeled to occur at the rate indicated by the blue asterisk in Figure 3, and gene gain and loss events were modeled to occur with twice the frequency indicated by the blue asterisk in Figure 4. Figure 5 Left gives the observed size distribution of gaps.

We then applied each aligner to the simulated genomes and measured the accuracy of gap predictions as a function of gap size. The aligners Mauve 1.3.0, MAVID 2.0, MLAGAN 2.0, TBA 28-02-2006, Progressive Mauve, and Pecan v0.7 were tested. Pecan v0.7 is a new aligner that has been demonstrated to have excellent performance (Margulies et al., 2007, Paten et al., 2008) by virtue of using probabilistic consistency during the anchoring process. Moreover, Pecan v0.7 uses a pair-HMM with an extra gap state specifically designed to model long indels. The reconstructed alignments were scored against the true alignments and results for ten replicates were recorded.

The right side of Figure 5 shows the quality of each aligner’s indel predictions as a function of the true gap size. Shown is the frequency with which gaps of a particular size are predicted as a single gap (singular TP) instead of a string of smaller gaps with interspersed alignments of

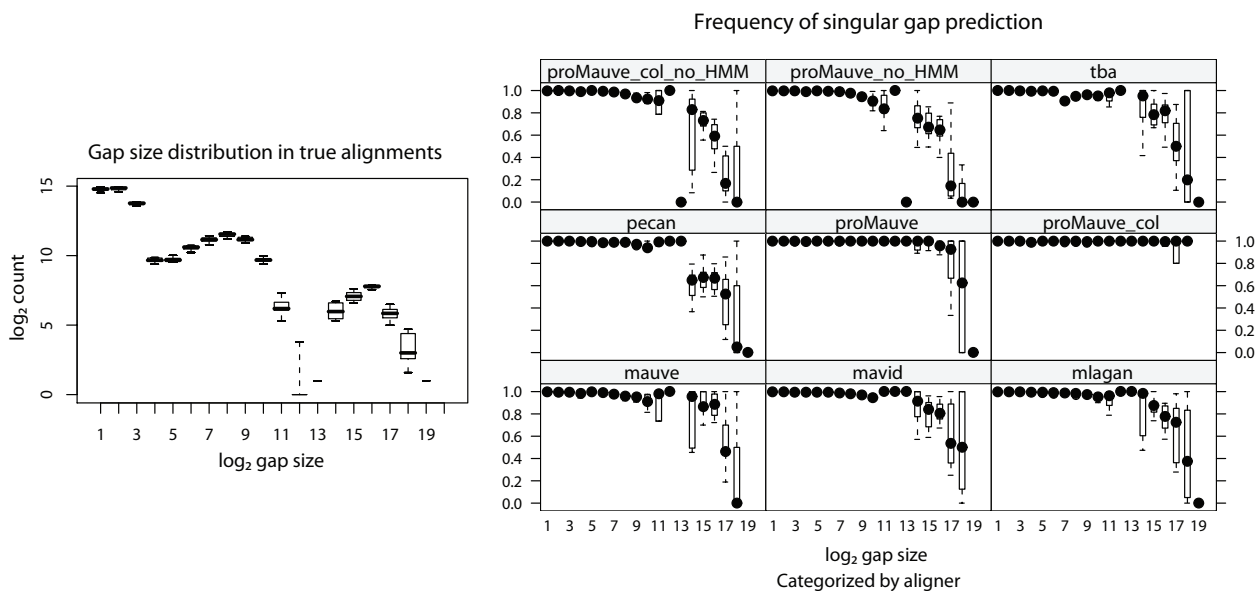


Figure 5: **Left** Average size distribution of gaps in an alignment of the nine genomes evolved at mutation rates which correspond to previous estimates for the *E. coli*, *Shigella*, and *Salmonella*. The gap size distribution was averaged over 10 simulations. **Right** Fraction of TP indel predictions that are singular TP indel predictions by true gap size. Ten replicate simulations of evolution with gene gain, gene loss, indels, and nucleotide substitution were performed and alignments were computed using each aligner. Predicted indels were classified according to the definitions given in Figure 2, namely, a singular True Positive implies the true gap is predicted as a single gap. Remaining True Positive indels have the true gap broken up into two or more predicted gaps. For each aligner, the fraction of singular predicted gaps is shown as a function of gap size. All aligners do well in predicting small gaps, but large gaps present problems. Most aligners, including Pecan which uses an extra pair-HMM state to model long gaps, tend to predict long gaps as a series of short gaps interspersed with alignments of unrelated sequence. We refer to such behavior as “gap dribble.” Progressive Mauve was run with default parameters (proMauve), without the Homology HMM (proMauve_no_HMM), with the option to assume genomes are collinear (proMauve_col), and finally assuming collinearity and without the HMM (proMauve_col_no_HMM).

non-homologous sequence (nonsingular TP). From the figure, it is obvious that aligners which use an affine gap penalty tend to perform poorly in predicting large gaps. Somewhat surprisingly, the pair-HMM with an extra gap state used by Pecan to model long indels still yields poor predictions of long gaps, although sensitivity is quite good (not shown). Progressive Mauve appears to perform well at all gap sizes, especially when the aligner is told to explicitly assume the genomes are collinear (proMauve_col). To determine whether Progressive Mauve’s performance results from its anchoring algorithm or use of the Homology HMM to reject alignments of unrelated sequence, we also tested Progressive Mauve without the Homology HMM, shown as panels proMauve_no_HMM and proMauve_col_no_HMM. Without the Homology HMM Progressive Mauve yields inferior results, indicating that the Homology HMM does indeed address the problem of gap dribble.

DISCUSSION

Progressive Mauve alignments enable a wide variety of downstream research. Here we illustrate some applications with an alignment of 23 complete *E. coli*, *Shigella* and *Salmonella* genomes. The alignment can be used to characterize the shared (core) and total (pan-genome) amount of sequence found in these species. In related work, we demonstrate a method to statistically infer the phylogenetic history of gene flux and identify sudden changes in the overall rate of gene flux in ancestral lineages (see Didelot *et al* joint submission with this manuscript). The alignment can also be used to extract variable sites for more traditional phylogenetic analyses. Finally, we demonstrate that Progressive Mauve identifies both conserved regulatory regions and hypervariable intergenic regions.

When applied to twenty-three *E. coli*, *Shigella*, and *Salmonella* genomes, the resulting alignment reveals a core genome of 2,675 segments conserved among all taxa, which account for an average of 2.46 Mbp of each genome. Between the core segments lie regions conserved among subsets of taxa and regions unique to individual genomes. By counting each core, unique, and subset segment exactly once, one constructs a total pan-genome that includes genes and intergenic regions alike. The 23 genomes have a pan-genome of 15.2 Mbp, approximately three times that of a single strain, indicating a tremendous degree of variability in both genic and intergenic content.

Shigella spp. are widely recognized as *E. coli* based phylogenetic analyses (Pupo *et al.*, 2000) and genome comparisons (Yang *et al.*, 2007), though the original phenotypically derived taxonomy persists. We will refer to them collectively as *E. coli/Shigella*. Similarly, taxonomic revisions of *Salmonella*, have collapsed almost all strains into a single species: *S. enterica*. Thus, we are examining the structure of the pan and core genomes of two sister species, *E. coli/Shigella* and *Salmonella*. The 16 *E. coli/Shigella* strains have a pan-genome of 12.5 Mbp and core of 2.9 Mbp, while the seven *S. enterica* serovars have a pan-genome of 5.8 Mbp and a core genome of 4.1 Mbp. The intersection of the core genomes is the joint core, while the union of the pan-genomes is the combined pan-genome, shown in Figure 6. Note that the intersection of pan-genomes is 580 kb larger than the joint core. This counter-intuitive situation arises when components of the core-genome of one group are found in some, but not all members of the other species. In this instance, 220 kb can be attributed to losses of genes in *Shigella* strains that are otherwise conserved among all *E. coli* and *Salmonella*. A more detailed dissection of the patterns of gene flux in the *E. coli/Shigella* lineage appears in the joint Didelot *et al* submission.

Inference of genome rearrangement history

Progressive Mauve alignments also make an excellent starting point for analysis of genome rearrangement patterns. Genome rearrangement is known to occur via a multitude of mutational forces, including inversion, transposition, and duplication/loss, and is especially prominent in bacterial pathogens. Methods already exist to infer inversion histories among pairs of genomes (Hannenhalli and Pevzner, 1995, Tannier and Sagot, 2004) and multiple genomes (Tang and Moret, 2003, Larget *et al.*, 2002). More general models to account for multiple chromosomes and multi-break rearrangements have also been developed (Yancopoulos *et al.*, 2005, Bergeron *et al.*, 2006, Alekseyev, 2008), although not yet in either phylogenetic or Bayesian contexts.

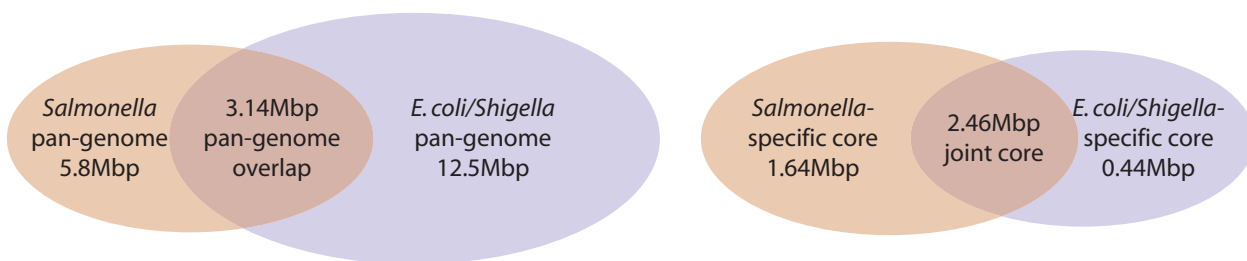


Figure 6: Venn diagram of the pan-genome (left) and core genome (right) of *E. coli/Shigella* and *S. enterica*.

Most genome rearrangement history inference methods do not also infer gene gain and loss, but instead assume that gene content across genomes is equal. When gene content is nearly equal, current models can use a multiple genome alignment to infer patterns of selection on genome rearrangement (Darling et al., 2008). However, equal gene content has proved to be the exception rather than the rule. Despite that, a Progressive Mauve alignment with differential content can be trivially reduced to contain only segments conserved among all taxa of interest, yielding a signed gene-order permutation matrix that is suitable for current genome rearrangement inference software.

Alignment visualization

Genome alignments are large and complex entities that are not usually suitable for direct interpretation. Genome comparison browsers such as the UCSC browser (Miller et al., 2007), VISTA (Mayor et al., 2000), and others have proven invaluable as tools to facilitate understanding of whole genome alignments. To aid in use of Progressive Mauve alignments, we have developed an interactive visualization program that can present a complex alignment in a meaningful and easily understandable visual paradigm.

The visualization system illustrates three major aspects of genome evolution: genome rearrangement, patterns of segmental gain and loss, and selective pressures for or against regional conservation of nucleotide sequences. Figure 7 illustrates two of these aspects in a visualization of the 23-way alignment of *E. coli*, *Shigella*, and *Salmonella*.

Figure 7 shows the region surrounding the *yhjE* gene, which encodes a product in the Major Facilitator Superfamily of transporters. *yhjE* is flanked by *yhjD* to the left, and *yhjG* to the right. The intergenic regions between these three genes are hypervariable (as indicated by the variety of colors in Figure 7) and have been subject to multiple insertion and deletion events. The hypervariable nature of the regions surrounding *yhjE* may not be surprising, because it harbors a REP element to the left, and a RIP element to the right. REP elements contain a series of two or more 35-bp palindromic repeats and are known for a variety of functions, including the binding of DNA gyrase and PolII, and as mRNA anti-decay hairpins or rho-dependent attenuators. RIP elements are a specialized form of REP elements that contain an IHF binding site, and this particular RIP also contains a REPt transcription terminator sequence. IHF is a global transcriptional regulator in *E. coli*.

Interestingly, the patterns of insertion/deletion in the intergenic regions surrounding *yhjE* do not follow the expected taxonomic patterns, suggesting instead that recombination among strains has taken place. The RIP region present to the right of *yhjE* in most *E. coli* has been replaced with an unrelated sequence in *E. coli* E23477A and *S. boydii* (shown as turquoise in Figure 7), but not in *S. sonnei*. Those three strains form a clade in the *E. coli/Shigella* taxonomy (Didot et al., 2008) with *E. coli* E23477A branching first, so convergent evolution must have occurred here.

The pattern of intergenic variability surrounding *yhjE* suggests potential regulatory divergence, a much studied evolutionary mechanism in eukaryotes largely overlooked in prokaryotic research. The *yhjE* locus is by no means the only region harboring intergenic variability; a screen of the 23-



Figure 7: A Mauve visualization of the hypervariable intergenic regions surrounding *yhdE*. Each genome is laid out in a horizontal track, with annotated coding regions shown as white boxes. A colored similarity plot is shown for each genome, the height of which is proportional to the level of sequence identity in that region. When the similarity plot points downward it indicates an alignment to the reverse strand of the genome. Colors in the similarity plot indicate the combination of organisms containing a particular segment of the genome. Segments colored pink/mauve are conserved among all organisms, while purple segments are conserved in everything but *Salmonella*, and segments colored in olive green are conserved among non-uropathogenic *E. coli*. The visualization system is interactive and written in Java, and works on all computers supporting Java 1.4 or later.

way alignment identifies 102 other strictly intergenic regions with similarly variable conservation patterns.

Conclusions

We have presented a novel multiple genome alignment heuristic which demonstrates a substantial accuracy improvement on simulated datasets. Key features of the approach are an anchor scoring function that penalizes alignment anchoring in repetitive regions of the genome and penalizes genomic rearrangement. Use of a Sum-of-pairs approach enables robust scoring of genomes that have undergone both gene flux and rearrangement—a scenario not addressed by previous alignment methods.

Future efforts to improve genome alignment may explicitly incorporate models of evolutionary distance into alignment scoring process (Fu et al., 2007). Multiple alignment methods based on probabilistic consistency have demonstrated great promise in the context of amino-acid alignment (Do et al., 2005) and aligning collinear genomic regions (Paten et al., 2008), and in principle, could be also extended to genome alignment with rearrangement.

No method reconstructs error-free genome alignments, and any particular alignment is likely to contain errors that can substantially influence downstream inference. However, methods to estimate the confidence in aligned columns are under continuing development (Lunter et al., 2008). Downstream inference methods that can explicitly cope with the inherent uncertainty in reconstructed alignments will be crucial for continued advances in comparative genomics.

ACKNOWLEDGEMENTS

We thank Eric Cabot, Anna Rissman, and Paul Infield-Harm for suggestions and contributions related to alignment visualization. Work supported in part by NIH R01-GM62994 to N.T.P. and NSF grant DBI-0630765 to A.E.D. This project has also been funded in part with Federal funds from the National Institute of Allergy and Infectious Diseases, National Institutes of Health, Department of Health and Human Services, under Contract No. HHSN266200400040C.

References

- Achaz, G., Coissac, E., Netter, P., and Rocha, E. P. (2003). Associations between inverted repeats and the structural evolution of bacterial genomes. *Genetics*, 164(4):1279–1289.
- Alekseyev, M. A. (2008). Multi-break rearrangements and breakpoint re-uses: from linear to circular genomes. *Journal of Computational Biology*.
- Bergeron, A., Mixtacki, J., and Stoye, J. (2006). A unifying view of genome rearrangements. In Bucher, P. and Moret, B. M. E., editors, *WABI '06: Proceedings of the Sixth International Workshop on Algorithms in Bioinformatics*, volume 4175 of *Lecture Notes in Computer Science*, pages 163–173. Springer.
- Blanchette, M., Bourque, G., and Sankoff, D. (1997). Breakpoint Phylogenies. *Genome Inform Ser Workshop Genome Inform*, 8:25–34.
- Blanchette, M., Kent, W. J., Riemer, C., Elnitski, L., Smit, Arian, F. A., Roskin, K. M., Baertsch, R., Rosenbloom, K., Clawson, H., Green, E. D., Haussler, D., and Miller, W. (2004). Aligning multiple genomic sequences with the threaded blockset aligner. *Genome Res*, 14(4):708–15.
- Bray, N. and Pachter, L. (2003). MAVID multiple alignment server. *Nucleic Acids Res*, 31(13):3525–6.
- Brudno, M., Do, Chuong, B., Cooper, Gregory, M., Kim, M. F., Davydov, E., Green, E. D., Sidow, A., and Batzoglou, S. (2003a). LAGAN and Multi-LAGAN: efficient tools for large-scale multiple alignment of genomic DNA. *Genome Res*, 13(4):721–31.
- Brudno, M., Malde, S., Poliakov, A., Do, Chuong, B., Couronne, O., Dubchak, I., and Batzoglou, S. (2003b). Glocal alignment: finding rearrangements during alignment. *Bioinformatics*, 19 Suppl 1:I54–I62.
- Chandra, R., Dagum, L., Kohr, D., Maydan, D., McDonald, J., and Menon, R. (2001). *Parallel programming in OpenMP*. Morgan Kaufmann Publishers Inc., San Francisco, CA, USA.
- Chao, K. M., Zhang, J., Ostell, J., and Miller, W. (1995). A local alignment tool for very long dna sequences. *Comput Appl Biosci*, 11(2):147–153.
- Chiaromonte, F., Yap, V. B., and Miller, W. (2002). Scoring pairwise genomic sequence alignments. *Pac Symp Biocomput*, pages 115–126.
- Darling, A. C. E., Mau, B., Blattner, F. R., and Perna, N. T. (2004a). Mauve: multiple alignment of conserved genomic sequence with rearrangements. *Genome Res*, 14(7):1394–403.
- Darling, A. E. (2006). *Computational Analysis of Genome Evolution*. PhD thesis, University of Wisconsin–Madison.
- Darling, A. E., Mau, B., Blattner, F. R., and Perna, N. T. (2004b). GRIL: Genome rearrangement and inversion locator. *Bioinformatics*, 20(1):122–124.

- Darling, A. E., Miklós, I., and Ragan, M. A. (2008). Dynamics of genome rearrangement in bacterial populations. *PLoS Genetics*.
- Darling, A. E., Treangen, T. J., Zhang, L., Kuiken, C., Messeguer, X., and Perna, N. T. (2006). Procrastination leads to efficient filtration for local multiple alignment. In *WABI 2006: Proceedings of the sixth annual Workshop on Algorithms in Bioinformatics*, volume 4175, pages 126–137, Germany. Springer Verlag.
- Dewey, C. N. and Pachter, L. (2006). Evolution at the nucleotide level: the problem of multiple whole-genome alignment. *Hum Mol Genet*, 15 Suppl 1.
- Didelot, X., Darling, A., and Falush, D. (2008). Inference of genomic flux in bacteria. *Joint Submission to Genome Research*.
- Do, C. B., Mahabhashyam, M. S., Brudno, M., and Batzoglou, S. (2005). ProbCons: Probabilistic consistency-based multiple sequence alignment. *Bioinformatics*, 15(2):330–340.
- Durbin, R., Eddy, S., Krogh, A., and Mitchison, G. (1998). *Biological Sequence Analysis*, chapter 4, pages 80–94. Cambridge University Press.
- Edgar, R. C. (2004). MUSCLE: a multiple sequence alignment method with reduced time and space complexity. *BMC Bioinformatics*, 5(1):113.
- Fitch, W. M. (2000). Homology: a personal view on some of the problems. *Trends Genet*, 16(5):227–231.
- Fu, Z., Chen, X., Vacic, V., Nan, P., Zhong, Y., and Jiang, T. (2007). Msoar: A high-throughput ortholog assignment system based on genome rearrangement. *Journal of Computational Biology*, 14(9):1160–1175.
- Hannenhalli, S. and Pevzner, P. A. (1995). Transforming men into mice (polynomial algorithm for genomic distance problem). In *FOCS '95: Proceedings of the 36th Annual Symposium on Foundations of Computer Science (FOCS'95)*, Washington, DC, USA. IEEE Computer Society.
- Henz, S., Huson, D., Auch, A. F., Nieselt-Struwe, K., and Schuster, S. (2005). Whole-genome prokaryotic phylogeny. *Bioinformatics*, 21(10):2329–2335.
- Hogg, J. S., Hu, F. Z., Janto, B., Boissy, R., Hayes, J., Keefe, R., Post, C. J., and Ehrlich, G. D. (2007). Characterization and modeling of the *Haemophilus influenzae* core- and supra-genomes based on the complete genomic sequences of Rd and 12 clinical nontypeable strains. *Genome Biology*, 8:R103+.
- Hohl, M., Kurtz, S., and Ohlebusch, E. (2002). Efficient multiple genome alignment. *Bioinformatics*, 18 Suppl 1:S312–20.
- Hsiao, W. W., Ung, K., Aeschliman, D., Bryan, J., Finlay, B. B., and Brinkman, F. S. (2005). Evidence of a large novel gene pool associated with prokaryotic genomic islands. *PLoS Genetics*, 1(5):e62+.
- Kucherov, G., Noe, L., and Roytberg, M. (2005). Multiseed lossless filtration. *IEEE/ACM Trans. Comput. Biol. Bioinformatics*, 2(1):51–61.
- Kumar, S. and Filipinski, A. (2007). Multiple sequence alignment: In pursuit of homologous DNA positions. *Genome Res.*, 17(2):127–135.
- Kurtz, S., Phillippy, A., Delcher, A. L., Smoot, M., Shumway, M., Antonescu, C., and Salzberg, S. L. (2004). Versatile and open software for comparing large genomes. *Genome Biol*, 5(2):R12.

- Larget, B., Simon, D. L., and Kadane, J. (2002). On a Bayesian approach to phylogenetic inference from animal mitochondrial genome arrangements. *Journal of the Royal Statistical Society, B* 64:681–693.
- Li, L., Stoeckert, C. J., and Roos, D. S. (2003). OrthoMCL: identification of ortholog groups for eukaryotic genomes. *Genome Res*, 13(9):2178–2189.
- Lippert, R. A., Zhao, X., Florea, L., Mobarry, C., and Istrail, S. (2004). Finding anchors for genomic sequence comparison. In *RECOMB '04: Proceedings of the eighth annual international conference on Research in computational molecular biology*, pages 233–241, New York, NY, USA. ACM Press.
- Lunter, G. (2007). Probabilistic whole-genome alignments reveal high indel rates in the human and mouse genomes. *Bioinformatics*, 23(13).
- Lunter, G., Rocco, A., Mimouni, N., Heger, A., Caldeira, A., and Hein, J. (2008). Uncertainty in homology inferences: Assessing and improving genomic sequence alignment. *Genome Res.*, 18(2):298–309.
- Ma, B., Tromp, J., and Li, M. (2002). PatternHunter: faster and more sensitive homology search. *Bioinformatics*, 18(3):440–5.
- Margulies, E. H., Cooper, G. M., Asimenos, G., Thomas, D. J., Dewey, C. N., Siepel, A., Birney, E., Keefe, D., Schwartz, A. S., Hou, M., Taylor, J., Nikolaev, S., Montoya-Burgos, J. I., Loytynoja, A., Whelan, S., Pardi, F., Massingham, T., Brown, J. B., Bickel, P., Holmes, I., Mullikin, J. C., Ureta-Vidal, A., Paten, B., Stone, E. A., Rosenbloom, K. R., Kent, J. W., Bouffard, G. G., Guan, X., Hansen, N. F., Idol, J. R., Maduro, V. V., Maskeri, B., McDowell, J. C., Park, M., Thomas, P. J., Young, A. C., Blakesley, R. W., Muzny, D. M., Sodergren, E., Wheeler, D. A., Worley, K. C., Jiang, H., Weinstock, G. M., Gibbs, R. A., Graves, T., Fulton, R., Mardis, E. R., Wilson, R. K., Clamp, M., Cuff, J., Gnerre, S., Jaffe, D. B., Chang, J. L., Lindblad-Toh, K., Lander, E. S., Hinrichs, A., Trumbower, H., Clawson, H., Zweig, A., Kuhn, R. M., Barber, G., Harte, R., Karolchik, D., Field, M. A., Moore, R. A., Matthews, C. A., Schein, J. E., Marra, M. A., Antonarakis, S. E., Batzoglou, S., Goldman, N., Hardison, R., Haussler, D., Miller, W., Pachter, L., Green, E. D., and Sidow, A. (2007). Analyses of deep mammalian sequence alignments and constraint predictions for 1% of the human genome. *Genome Res.*, 17(6):760–774.
- Mau, B., Glasner, J. D., Darling, A. E., and Perna, N. T. (2006). Genome-wide detection and analysis of homologous recombination among sequenced strains of *Escherichia coli*. *Genome Biology*, 7:R44+.
- Mayor, C., Brudno, M., Schwartz, J. R., Poliakov, A., Rubin, E. M., Frazer, K. A., Pachter, L. S., and Dubchak, I. (2000). Vista : visualizing global dna sequence alignments of arbitrary length. *Bioinformatics (Oxford, England)*, 16(11):1046–1047.
- Miller, W., Rosenbloom, K., Hardison, R. C., Hou, M., Taylor, J., Raney, B., Burhans, R., King, D. C., Baertsch, R., Blankenberg, D., Kosakovsky, Nekrutenko, A., Giardine, B., Harris, R. S., Tyekucheva, S., Diekhans, M., Pringle, T. H., Murphy, W. J., Lesk, A., Weinstock, G. M., Lindblad-Toh, K., Gibbs, R. A., Lander, E. S., Siepel, A., Haussler, D., and Kent, J. W. (2007). 28-Way vertebrate alignment and conservation track in the UCSC Genome Browser. *Genome Res.*, pages gr.6761107+.
- Ogurtsov, A. Y., Roytberg, M. A., Shabalina, S. A., and Kondrashov, A. S. (2002). Owen: aligning long collinear regions of genomes. *Bioinformatics*, 18(12):1703–1704.
- Ovcharenko, I., Loots, G. G., Giardine, B. M., Hou, M., Ma, J., Hardison, R. C., Stubbs, L., and Miller, W. (2005). Mulan: Multiple-sequence local alignment and visualization for studying function and evolution. *Genome Res*, 15(1):184–94.

- Paten, B., Beal, K., and Birney, E. (2008). Pecan: Large-scale consistency alignment. *Unpublished draft*.
- Perna, N. T., Plunkett, G., Burland, V., Mau, B., Glasner, J. D., Rose, D. J., Mayhew, G. F., Evans, P. S., Gregor, J., Kirkpatrick, H. A., Posfai, G., Hackett, J., Klink, S., Boutin, A., Shao, Y., Miller, L., Grotbeck, E. J., Davis, N. W., Lim, A., Dimalanta, E. T., Potamousis, K. D., Apodaca, J., Anantharaman, T. S., Lin, J., Yen, G., Schwartz, D. C., Welch, R. A., and Blattner, F. R. (2001). Genome sequence of enterohaemorrhagic *Escherichia coli* O157:H7. *Nature*, 409(6819):529–33.
- Phuong, T. M., Do, C. B., Edgar, R. C., and Batzoglou, S. (2006). Multiple alignment of protein sequences with repeats and rearrangements. *Nucleic Acids Res.*, 34:5932–42.
- Prakash, A. and Tompa, M. (2007). Measuring the accuracy of genome-size multiple alignments. *Genome Biology*, 8:R124+.
- Pupo, G. M., Lan, R., and Reeves, P. R. (2000). Multiple independent origins of *Shigella* clones of *Escherichia coli* and convergent evolution of many of their characteristics. *Proc Natl Acad Sci U S A*, 97:10567–72.
- Raphael, B., Zhi, D., Tang, H., and Pevzner, P. (2004). A novel method for multiple alignment of sequences with repeated and shuffled elements. *Genome Res*, 14(11):2336–46.
- Swidan, F., Rocha, E. P. C., Shmoish, M., and Pinter, R. Y. (2006). An integrative method for accurate comparative genome mapping. *PLoS Comput Biol*, 2(8).
- Tang, J. and Moret, B. M. (2003). Scaling up accurate phylogenetic reconstruction from gene-order data. *Bioinformatics*, 19 Suppl 1:i305–i312.
- Tannier, E. and Sagot, M.-F. (2004). Sorting by reversals in subquadratic time. In *Lecture Notes in Computer Science*, volume 3109, pages 1–13. Springer-Verlag.
- Tettelin, H., Maignani, V., Cieslewicz, M. J., Donati, C., Medini, D., Ward, N. L., Angiuoli, S. V., Crabtree, J., Jones, A. L., Durkin, A. S., Deboy, R. T., Davidsen, T. M., Mora, M., Scarselli, M., Margarit y Ros, I., Peterson, J. D., Hauser, C. R., Sundaram, J. P., Nelson, W. C., Madupu, R., Brinkac, L. M., Dodson, R. J., Rosovitz, M. J., Sullivan, S. A., Daugherty, S. C., Haft, D. H., Selengut, J., Gwinn, M. L., Zhou, L., Zafar, N., Khouri, H., Radune, D., Dimitrov, G., Watkins, K., O’Connor, K. J., Smith, S., Utterback, T. R., White, O., Rubens, C. E., Grandi, G., Madoff, L. C., Kasper, D. L., Telford, J. L., Wessels, M. R., Rappuoli, R., and Fraser, C. M. (2005). Genome analysis of multiple pathogenic isolates of *Streptococcus agalactiae*: implications for the microbial “pan-genome”. *Proc Natl Acad Sci U S A*, 102(39):13950–13955.
- Thompson, J. D., Plewniak, F., and Poch, O. (1999). A comprehensive comparison of multiple sequence alignment programs. *Nucleic Acids Res*, 27(13):2682–90.
- Treangen, T. J., Darling, A. E., Ragan, M. A., and Messeguer, X. (2008). Gapped extension for local multiple alignment of interspersed repeats. In *Proceedings of ISBRA 2008: Bioinformatics Research and Applications*, pages 74–86, Heidelberg, Germany. Springer-Verlag Berlin.
- Treangen, T. J. and Messeguer, X. (2006). M-GCAT: Interactively and efficiently constructing large-scale multiple genome comparison frameworks in closely related species. *BMC Bioinformatics*, 7:433+.
- Vernikos, G. S., Thomson, N. R., and Parkhill, J. (2007). Genetic flux over time in the *Salmonella* lineage. *Genome Biology*, 8:R100+.
- Vinh, L. S., Varon, A., and Wheeler, W. C. (2006). Pairwise alignment with rearrangements. *Genome Inform*, 17(2):141–151.

- Welch, R. A., Burland, V., Plunkett, G., Redford, P., Roesch, P., Rasko, D., Buckles, E. L., Liou, S.-R., Boutin, A., Hackett, J., Stroud, D., Mayhew, G. F., Rose, D. J., Zhou, S., Schwartz, D. C., Perna, N. T., Mobley, H. L. T., Donnenberg, M. S., and Blattner, F. R. (2002). Extensive mosaic structure revealed by the complete genome sequence of uropathogenic *Escherichia coli*. *Proc Natl Acad Sci U S A*, 99(26):17020–4.
- Yancopoulos, S., Attie, O., and Friedberg, R. (2005). Efficient sorting of genomic permutations by translocation, inversion and block interchange. *Bioinformatics*, 21(16):3340–3346.
- Yang, J., Nie, H., Chen, L., Zhang, X., Yang, F., Xu, X., Zhu, Y., Yu, J., and Jin, Q. (2007). Revisiting the molecular evolutionary history of *Shigella* spp. *J Mol Evol.*, 64:71–9.

APPENDIX

Organism	Genome size w/Plasmids	Accession
<i>E. coli</i> K-12 MG1655	4,654,221	U00096
<i>E. coli</i> K-12 W3110	4,646,332	AP009048
<i>E. coli</i> HS	4,643,538	AAJY00000000
<i>E. coli</i> O157:H7 EDL933	5,623,806	AE005174
<i>E. coli</i> O157:H7 Sakai	5,594,477	BA000007
<i>E. coli</i> E24377A	4,980,187	AAJZ00000000
<i>E. coli</i> CFT073 (UPEC)	5,231,428	AE014075
<i>E. coli</i> UTI89 (UPEC)	5,179,971	CP000243
<i>E. coli</i> APEC O1	5,082,025	CP000468
<i>E. coli</i> 536 (UPEC)	4,938,920	CP000247
<i>Shigella boydii</i> Sb227	4,646,520	CP000036
<i>Shigella flexneri</i> 2a 2457T	4,988,914	AE014073
<i>Shigella flexneri</i> 2a 301	4,828,821	AE005674
<i>Shigella flexneri</i> 5 8401	4,574,284	CP000266
<i>Shigella dysenteriae</i> Sd197	4,551,958	CP000034
<i>Shigella sonnei</i> Ss046	5,039,661	CP000038
<i>Salmonella enterica</i> Choleraesuis B67	4,944,000	AE017220
<i>Salmonella enterica</i> Typhi Ty2	4,791,961	AE014613
<i>Salmonella enterica</i> Typhi CT18	5,133,713	AL513382
<i>Salmonella enterica</i> Typhimurium LT2	4,951,371	AE006468
<i>Salmonella enterica</i> Paratyphi A ATCC9150	4,585,229	CP000026
<i>Salmonella enterica</i> Arizonae	4,600,800	NC_010067
<i>Salmonella enterica</i> Paratyphi B SPB7	4,858,887	NC_010102

Table 1: **(Supplementary)** Twenty-three publicly-available, finished genome sequences from the genera *Salmonella*, *Escherichia*, and *Shigella* form our target set for multiple genome alignment.

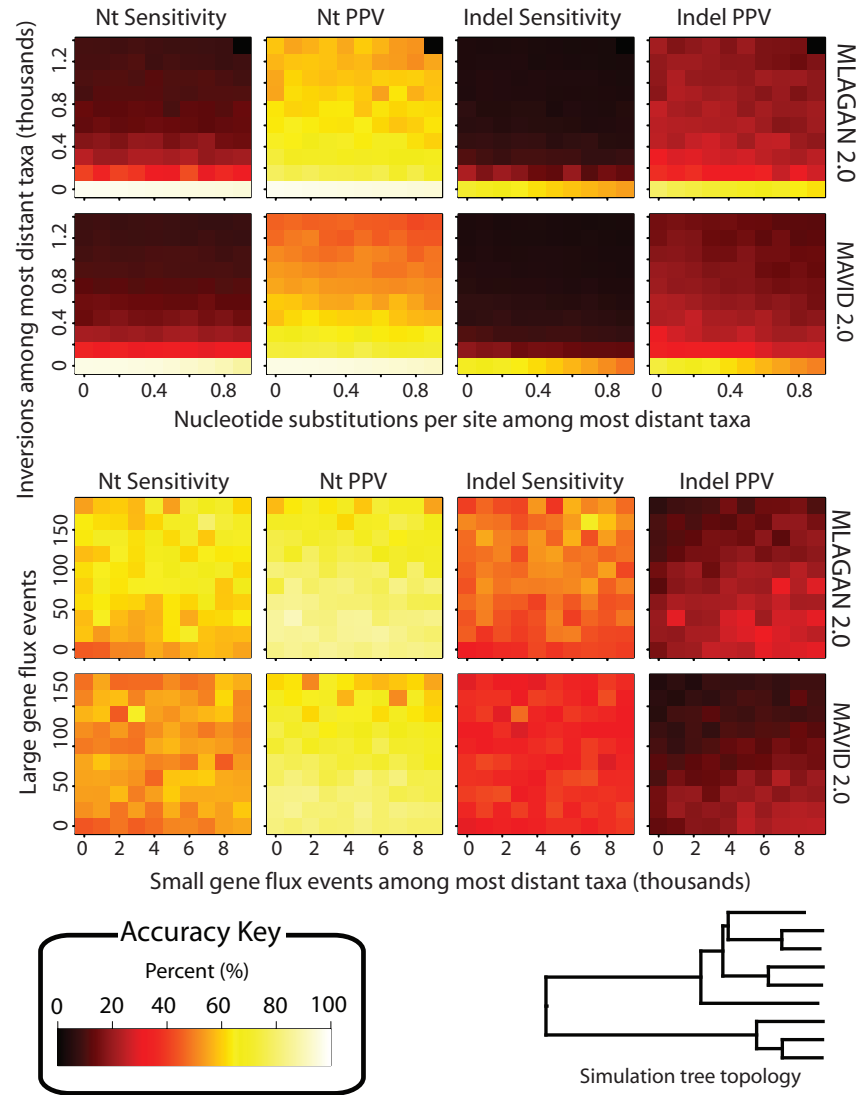


Figure 8: **Supplementary** The performance of MLAGAN 2.0 and MAVID 2.0 on genomes evolved with inversions, gene gain, and gene loss corresponding to Figure 4. Neither MLAGAN nor MAVID were designed to align genomes with rearrangement and differential content; this figure demonstrates the decay in alignment quality when such forces are present in the data but not modeled by the aligner. The black dot in the upper right corner of the MLAGAN results indicates that MLAGAN did not finish alignments at the highest combination of inversion and substitution rate within the allotted 10 hour limit.